ELSEVIER

Materials Science and Engineering A 399 (2005) 107–113

MATERIALS SCIENCE & ENGINEERING A

www.elsevier.com/locate/msea

Residual stresses in a bulk metallic glass–stainless steel composite

C.C. Aydıner [a], E. Üstündag [a,*], B. Clausen [c], J.C. Hanan [b,1], R.A. Winholtz [d], M.A.M. Bourke [e], A. Peker [f]

[a] *Department of Materials and Science Engineering, Iowa State University, Ames, IA 50011, USA*
[b] *Division of Engineering and Applied Science, California Institute of Technology, Pasadena, CA 91125, USA*
[c] *Lujan Neutron Science Center, Los Alamos National Laboratory, Los Alamos, NM 87545, USA*
[d] *Department of Mechanical and Aerospace Engineering and Research Reactor Center, University of Missouri, Columbia, MO 65211, USA*
[e] *Materials Science and Technology Division, Los Alamos National Laboratory, Los Alamos, NM 87545, USA*
[f] *Liquidmetal Technologies, Lake Forest, CA 92630, USA*

Abstract

Bulk metallic glasses (BMGs) are new structural materials with impressive mechanical properties. They can now be cast into large dimensions, which can lead to significant residual stress generation due to thermal tempering. In this process, a surface compression develops balanced with tension in the interior. To evaluate this phenomenon non-destructively, a model cylindrical stainless steel (SS)–BMG composite was prepared and studied using neutron diffraction and finite element (FE) modeling. The residual strain data from the SS obtained by diffraction were used in modeling calculations to show that significant tempering could be achieved in the composite (about −200 MPa surface compression in the SS). The strong bond between the SS and BMG allowed efficient load transfer and facilitated stress generation. The final values of the residual stresses were seen to be relatively insensitive to the high temperature constitutive behavior of the SS due to the physics of the thermal tempering in BMGs. The approach presented here constitutes an effective means to study non-destructively thermal tempering in BMGs.

Keywords: Neutron diffraction; Metallic glass; Thermal tempering; Residual stress; Finite element modeling; Strain measurement

1. Introduction

Although metallic glasses have been made since 1960, specimen dimensions were previously limited to tens of μm due to the very fast cooling rates (about 10^6 K/s) needed in order to prevent crystallization. Recently, multicomponent alloys have been developed with exceptional glass formation ability that allows the processing of *bulk* specimens as large as 50 mm in diameter [1]. Called bulk metallic glasses (BMGs), these new amorphous alloys exhibit impressive properties as structural materials: yield strength around 2 GPa, fracture toughness between 20 and 140 MPa $m^{1/2}$, elastic strain limit around 2%, good corrosion resistance and high specific strength [2].

Large specimen dimensions have introduced an important source of residual stress in BMGs due to the thermal tempering phenomenon. Thermal tempering refers to the generation of compressive residual stresses at the surface of glass specimens due to rapid cooling during processing. This is a well-established process in silicate glasses [3]. Thermal tempering in BMGs has been recently investigated for the first time by Aydiner et al. in a series of systematic studies [4–6]. Aydiner et al. showed that the thermoviscoelastic model they developed earlier can predict residual stresses within 15–30% of experimental data [6]. In these studies, the residual stresses were measured with the slitting (crack compliance) method [5,6], which offered good accuracy and spatial resolution. However, this is a destructive method that relies on measurement of mechanical relaxation caused by judicious material removal.

Residual stresses in BMGs are difficult to measure directly with non-destructive methods. The amorphous nature of BMGs precludes the commonly used diffraction-based

* Corresponding author. Tel.: +1 515 294 9678; fax: +1 515 294 7202.
E-mail address: ustundag@iastate.edu (E. Üstündag).
[1] Present address: Bio-Inspired Technologies and Systems, Jet Propulsion Laboratory, Pasadena, CA 91109, USA.

0921-5093/$ – see front matter © 2005 Elsevier B.V. All rights reserved.
doi:10.1016/j.msea.2005.02.031

technique for residual stress measurement. However, it is possible to introduce a limited amount of crystalline phase into the BMG alloy and measure the residual elastic strain in it after processing. Then, the link between the strains measured in the crystalline phase and the stresses in the BMG can be established through mechanical modeling. This approach has been successfully employed in studying the in situ deformation behavior of BMG matrix composites with metallic inclusions [7–13].

A similar approach is followed in the present study. A model cylindrical composite sample was produced under controlled conditions to evaluate the residual stresses in a BMG alloy. Due to its good interface strength and limited reactivity with most BMGs, stainless steel (SS) was used as the crystalline second phase. The residual strains in the steel were measured by neutron diffraction and compared with the results of a finite element (FE) analysis. It is shown that significant residual stresses are induced in the SS–BMG composite and that neutron diffraction and FE can be effectively combined to evaluate and predict them.

2. Experimental procedure

2.1. Sample preparation

The sample geometry is shown in Fig. 1. It consists of an AISI 314 stainless steel pin at the center (diameter: 3.2 mm), a tube of the same steel at the circumference (outer diameter: 19.0 mm and inner diameter: 15.6 mm) and a BMG alloy (Vitreloy 1: $Zr_{41.2}Ti_{13.8}Cu_{12.5}Ni_{10.0}Be_{22.5}$) in between. The first step in the production of this specimen was the welding of a SS pin to the closed end of a 900-mm long SS tube. Next, the top end of the tube was connected to a vacuum line after pre-cast BMG ingots were put inside. The assembly was evacuated and placed in a vertical furnace where the BMG alloy melted at around 900 °C and filled the volume between the pin and the tube. Finally, the composite was quenched in room temperature water. A 50-mm long section of the SS–BMG composite was then cut to obtain the specimen in Fig. 1. Other details of specimen preparation using this method were presented elsewhere [1,6]. It is important to note that both SS–BMG interfaces were intact after processing. An identical tube (with an attached pin) was also heat treated under the same conditions, but without a BMG core, to be used as a stress-free reference in neutron diffraction measurements.

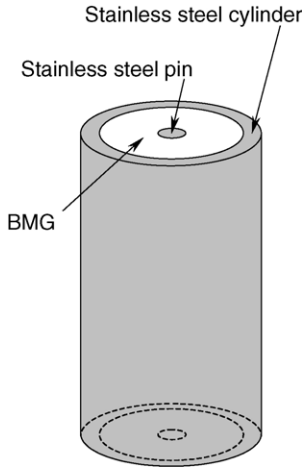

Fig. 1. Model specimen made of a type-314 stainless steel tube (19.0 mm outer diameter and 15.6 mm inner diameter) and a middle pin (3.2 mm diameter) with a Vitreloy 1 ($Zr_{41.2}T_{13.8}Cu_{12.5}Ni_{10}Be_{22.5}$) BMG cast in between. The specimen height is about 50 mm.

An accurate estimate of the heat transfer coefficient is crucial for a successful prediction of tempering-induced residual stresses. In this study, heat transfer during water quenching is assumed to obey the typical convective heat transfer relation: $Q = h(T_s - T_f)$, where Q is the heat flux, T_s the surface temperature of the specimen, T_f the temperature of the coolant fluid and h is the heat transfer coefficient. Since it is experimentally unfeasible to directly monitor the temperature evolution on the outer surface of the composite [6], a thermocouple-embedded SS rod (diameter: 12.7 mm and length: 101.6 mm) was used to deduce the value of the heat transfer coefficient by quenching it under identical conditions. The thermocouple, which is at the center of the rod's cross-section at mid-length, yields the temperature evolution at that location. To determine the heat transfer coefficient, first, the problem was solved for a range of assumed heat transfer coefficients. Then, the temperature history output of these calculations at the thermocouple location was compared with the experimental data. The best match between the two yields the heat transfer coefficient of the quench. The reader is referred to [6] for the mathematical implementation of this procedure and further experimental details. In the present study, additional experiments where the quench water was stirred with varied speeds showed that heat transfer is very weakly dependent on stream velocity (plausibly due to boiling convection [14]) and that the heat transfer coefficient varies between 8000 and 10,000 W/(m^2 K) with an average value of $h = 9000$ W/(m^2 K). These numbers were used in the FE calculations described later.

2.2. Residual strain measurement via neutron diffraction

Neutron diffraction provided a non-destructive measure of the residual strains in the steel components. The use of this technique at a reactor source and specifically at the Missouri University Research Reactor Center's 2XD powder diffractometer is described elsewhere [15,16]. Measurements were performed using a monochromatic neutron beam of wavelength, $\lambda = 1.478$ Å and a position sensitive detector (PSD). The 311 stainless steel peak at $2\theta = 86.6°$ was employed. The gage volume was a rectangular box of 1 mm × 1 mm × 8 mm defined by incident and diffracted beam slits (see Fig. 2). An oscillating radial collimator was used on the diffracted beam to reduce sources of background neutrons. The residual strain was obtained from the difference in the 311 lattice spacings

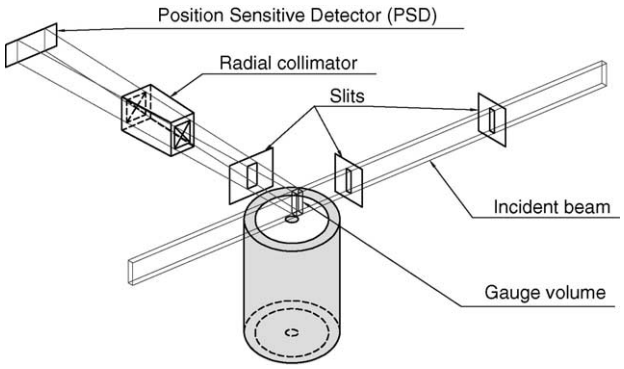

Fig. 2. Schematic of the 2XD neutron diffractometer at the Missouri University Research Reactor Center. The sampling (or gauge) volume is defined by slits in the incident and diffracted beams to be about 1 mm × 1 mm × 8 mm.

of the composite and the stress-free reference sample. The uncertainty in experimental strain data (obtained from four repeated measurements on the reference sample) is estimated at ± 330 με (where $\mu\varepsilon = 10^{-6}$ strain), mostly due to the translation error.

3. Modeling

3.1. Constitutive behavior of metallic glass and stainless steel

The thermoviscoelastic model that was previously developed [5] and shown to be reasonably accurate in comparison with experimental data [6] was used here to describe the constitutive behavior of BMG. The previous study [6] employed a monolithic cylindrical BMG sample. There, the error between the model predictions and experimental results varied along the sample radius, increasing from 15% at the center to 30% at the surface. This is typical of thermal tempering [17], where the temperature gradients at the surface are much higher during processing. In this model, as in the classical viscoelastic theory of tempering [18], the viscoelastic response is attributed to shear only and bulk deformation is assumed to be elastic. The shear relaxation modulus at a temperature T (G_T) is deduced from the equilibrium viscosity data, which is successfully fit with the Vogel–Fulcher–Tammann (VFT) relation [19]:

$$\eta(T) = \eta_0 \exp\left(\frac{D^* T_0}{T - T_0}\right) \quad (1)$$

where D^* is called the fragility parameter (18.5 for the $Zr_{41.2}Ti_{13.8}Cu_{12.5}Ni_{10}Be_{22.5}$ BMG alloy), $\eta_0 = 4 \times 10^{-5}$ Pa s, and T_0 is the VFT kinetic freezing temperature (412.5 K). The viscoelastic relation,

$$\eta(T) = \int_0^\infty G_T(t)\,\mathrm{d}t \quad (2)$$

allows the determination of the relaxation modulus from viscosity only if the functional form of G_T is known. Therefore,

Table 1
Thermophysical properties of stainless steel (AISI 314) and Vitreloy 1 ($Zr_{41.2}Ti_{13.8}Cu_{125}Ni_{10}Be_{22.5}$) metallic glass employed in the present study

Material	AISI 314 stainless steel [20]	$Zr_{41.2}Ti_{13.8}Cu_{12.5}Ni_{10}Be_{22.5}$ glass
Young's modulus, E (GPa)	193	96 [23]
Poisson's ratio, ν	0.30	0.36 [23]
Density, ρ (kg/m^3)	7800	6000 [24]
Thermal conductivity, k (W/(m K))	16.7 at 273 K	
	17.5 at 373 K	6.0 at 273 K
	20.9 at 773 K	18.8 at 1273 K [25]
	25.2 at 1273 K	
Specific heat, C_p (J/(kg K))		23 at 298 K
		28 at 600 K
		800 at 673 K
		740 at 773 K
	500	703 at 873 K
		681 at 973 K
		668 at 1073 K
		661 at 1173 K [26,27]
Coefficient of thermal expansion, α ($\times 10^{-6}$ K^{-1})	15.1	10.0 [24]

Aydiner et al. performed a parametric study to show that the predicted final residual stress state is practically independent of the shape of the relaxation modulus [5]. Hence, the simple Debye relaxation was employed in the present calculations:

$$G_T(t) = \mu_T \exp\left[-\frac{t}{\tau(T)}\right] \quad \text{where,} \quad \tau(T) = \frac{\eta(T)}{\mu_T} \quad (3)$$

Here, t is the time and μ_T is the instantaneous shear modulus at temperature T and $\tau(T)$ is the relaxation time. The reader is referred to [5] for further details of the viscoelastic model and how it is implemented in a finite element calculation.

The constitutive behavior of the AISI 314 stainless steel is given in Table 1 (elastic constants) and in Table 2 (plasticity data). It is well known that the plastic behavior of stainless steels is strongly dependent on heat treatment, sample dimen-

Table 2
Temperature dependent plastic behavior of AISI 314 stainless steel for the three cases considered

	Temperature (K)	σ_Y (MPa)	$\sigma_{T,Tensile}$ (MPa), $\varepsilon_{T,p}$
Case 1 [20]	298	205	721, 0.332
Case 2 [20]	298	310	868, 0.332
	294	358	1105, 0.498
	700	276	804, 0.346
	811	248	758, 0.355
Case 3 [21]	866	224	665, 0.297
	1033	138	450, 0.530
	1089	103	259, 0.407
	1144	90	274, 0.575

σ_Y: Yield strength, $\sigma_{T,Tensile}$: true stress at the ultimate tensile strength, and $\varepsilon_{T,p}$: the corresponding plastic component of true strain.

sions and geometry. As a result, a wide range of plasticity data exists for the AISI 314 steel. Therefore, the constitutive behavior of the SS was regarded a parameter in the present analysis and three data sets were considered. As will be shown, such a parametric study also helps with the understanding of the model predictions' sensitivity to the constitutive behavior of the SS, which could not be determined in situ during this investigation. The first two cases listed in Table 2 are room temperature test results whereas the third case includes high temperature data as well [20,21]. The data are presented in Table 2 in terms of yield strength (σ_Y), true stress at the ultimate tensile strength ($\sigma_{T,Tensile}$) and the corresponding plastic component of true strain ($\varepsilon_{T,P}$), the way they were used in the FE calculations. The latter two quantities specify the hardening behavior. The analysis assumed von Mises plasticity with isotropic hardening.

3.2. Finite element model

A sequential thermal-displacement analysis was employed to simulate the quenching problem in ABAQUS^{TM} finite element software [22]. In this analysis, first, the heat transfer problem was solved and nodal temperatures as a function of position and time were determined. The mechanical problem was then solved using the same mesh imposed by the previous temperature solution. Such an analysis assumes that the mechanical problem is not coupled to the heat transfer problem, which is reasonable since heat dissipation due to inelastic processes is overwhelmed by the severe cooling imposed during quenching.

The entire sample was modeled as a two-dimensional axis-symmetric mesh shown in Fig. 3(a). Quadratic elements were used for all calculations. The boundary condition for the heat transfer problem was uniform convective heat transfer from the circumference and the thermophysical data used for both phases are given in Table 1. The heat loss from the bottom of the tube was ignored due to the high aspect ratio of the sample. In addition, uniform cooling from the bottom, on its own, does not create thermal gradients in the radial direction, which are responsible for thermal tempering.

The mechanical problem was solved in a *VISCO step in ABAQUS^{TM} [22] that is used for stress/displacement analysis with time dependent material response (e.g., rate dependent plasticity and viscoelasticity). The *VISCO procedure implements time integration of material behavior in consecutive temporal increments. In each of these increments, iterations were carried out until convergence to quasi-static equilibrium was achieved. Here, the NLGEOM option of ABAQUS^{TM} [22] was used which allows large displacements by accounting for geometric non-linearity due to distortion of the mesh. It proved crucial in this analysis due to the large thermal contraction and bulging of the BMG (which acts as a fluid in the initial stages of the cooling process) that is squeezed by the stainless steel tube, which cools faster, and contracts with a larger coefficient of thermal expansion (see Table 1). The boundary conditions were chosen to approximate the conditions in the process and are shown in Fig. 3(a): zero traction on the circumference that is force-free and zero radial displacement along the center line due to axis-symmetry. In addition, zero traction on the top surface was assumed. This is fully justified for the BMG and pin (which constitute the majority of the sample cross-section) that have vacuum above them during processing, and is a simplifying assumption for the tube that is intact at that lo-

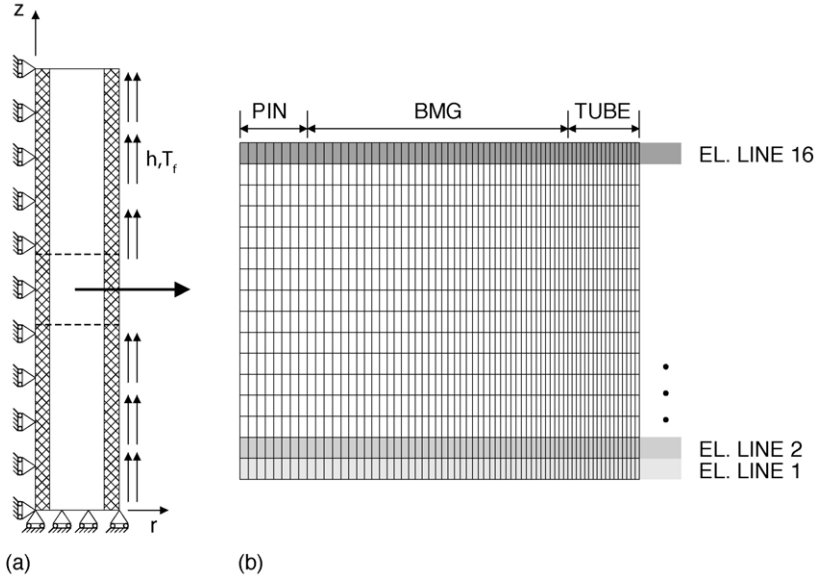

Fig. 3. (a) The two-dimensional, axis-symmetric finite element mesh with boundary conditions of thermal and mechanical analyses superimposed. The stainless steel section is cross-hatched whereas the BMG section is blank and (b) magnified view of the mid-section where the neutron sampling volume is placed along the axial direction. Model predictions are gathered along sixteen element lines in the radial direction that cover this region.

cation. The bottom of the sample was assumed to deform uniformly in the axial direction and was assigned a zero axial displacement boundary condition at the bottom surface.

The FE model consisted of a single mesh with elements assigned SS or BMG constitutive behavior at the corresponding sections. This means a "perfect" bond between the BMG and SS was assumed at all times. The intact SS–BMG interface observed after quenching justifies this assumption. In addition, the neutron diffraction results presented in the next section proved that the pin–BMG interface was strong after the solidification of the BMG since the pin was put under considerable tensile radial and axial stress. In other words, despite the existence of significant tensile stresses at the SS–BMG interfaces, they appear to build enough strength to withstand these stresses, especially after the solidification of the BMG when the majority of the stress generation occurs.

For a long cylinder geometry with uniform cooling, it was admissible in a previous study [6] to constrain the deformation in the axial direction to be uniform (generalized plane strain) so that the problem could be one-dimensional. In FE implementation of this type of modeling, only one line of elements are considered in the radial direction whose top nodes are constrained to deform uniformly in the axial direction. Such an analysis proved to be incorrect in the present study due to the existence of the SS pin. The uniform axial displacement constraint across the entire cross-section directly links the SS tube and pin before the metallic glass between them solidifies. Since the contraction of the rapidly cooled tube is very different from the pin at this stage, forcing them to deform equally creates large unphysical thermal stresses in both. Therefore, the generalized plane strain assumption was avoided in the present study and the entire specimen was modeled.

To allow a direct comparison with the diffraction data, the 8-mm long sampling volume was represented with 16 elements in the axial direction around the middle of the sample (see Fig. 3(b)). Stress and elastic strain values were gathered along these element lines in the radial direction and averaged in the axial direction to simulate the averaging by neutrons. Note that, as expected from the long cylinder geometry, the variation of stress and strain in the axial direction was found to be very low. Therefore, the results presented in the Section 4 may be viewed as representative of the mid-section of the sample.

4. Results and discussion

Axial elastic strain results from neutron diffraction and five different FE model predictions are presented in Fig. 4. In all but one FE model (namely, "Elastic SS, BMG (CTE)"), the constitutive behavior of the BMG was described by the thermoviscoelastic model presented in Section 3. In the latter case, both SS and BMG were considered linear elastic and no thermal gradients were allowed. Therefore, the only residual stress source in this case is the CTE mismatch between the

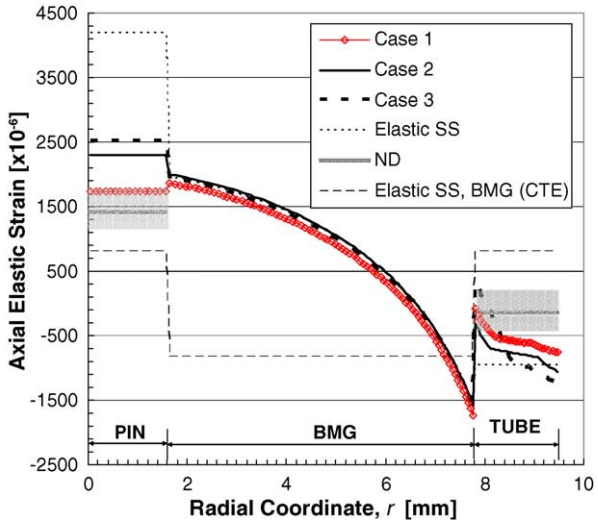

Fig. 4. Axial elastic strains measured by neutron diffraction (ND) and calculated for different constitutive behaviors of stainless steel (SS) and BMG: Case 1: $(\sigma_Y)_{SS} = 205$ MPa, BMG viscoelastic; Case 2: $(\sigma_Y)_{SS} = 310$ MPa, BMG viscoelastic; Case 3: $(\sigma_Y)_{SS} = 358$ MPa at room temperature and drops at higher temperatures (Table 2), BMG viscoelastic; "Elastic SS": SS linear elastic, BMG viscoelastic; "Elastic SS, BMG (CTE)" both phases are linear elastic, no thermal gradients allowed (CTE mismatch is the only residual stress source). The shaded areas represent the error bars for the ND data ($\pm 330\,\mu\varepsilon$).

two phases below 352 °C (the glass transition temperature of BMG). This case was considered to highlight the effect of temperature gradients in the residual stress state of the composite. It is obvious in Fig. 4 that if CTE mismatch were the only source of residual strain in this composite, then the axial strains in the pin and the tube would be identical and quite different than the experimental data. In all the other four FE models, the BMG behaved as a viscoelastic material, but the constitutive behavior of the SS varied from a linear elastic material ("Elastic SS"), to one with a room temperature yield strength of $\sigma_Y = 205$ MPa (Case 1), or $\sigma_Y = 310$ MPa (Case 2), and finally for Case 3, with a high yield strength at room temperature, $\sigma_Y = 358$ MPa which decreases at higher temperatures (see Table 2 for additional details). Note that the first two cases assume no variation of SS yield strength as a function of temperature.

Diffraction data exhibited a high tensile residual strain in the SS pin ($+1420\,\mu\varepsilon$) and a low compressive strain in the tube ($-140\,\mu\varepsilon$), both in the axial direction. A straight line was used to show the ND result for clarity although the measurement was taken from one location, 1 mm wide in the radial and hoop directions. The measurement in the pin is insensitive to the exact radial location of the sampling volume since the model calculations yielded almost uniform elastic strain in it. The variation in the tube is much more pronounced. The primary reason is that the pin, being at the center, never experienced severe temperature gradients within itself. When it yielded, plastic deformation was uniform and due to the loads exerted by the remaining section of the sample. Conversely, the tube underwent non-uniform plastic deformation even

before metallic glass solidified due to high thermal gradients within its wall. Such deformation was especially pronounced in Case 3 where high temperature softening of SS was considered. Note that when plastic deformation was prevented (the "Elastic SS" case), the strain distribution in the tube, too, became uniform (Fig. 4).

The ND data from the pin had a better signal-to-noise ratio. In addition, since the pin carries uniform axial strain, it is more advantageous in comparing the experimental data with model predictions. Therefore, the following discussion will concentrate only on the pin. When the FE calculations are compared with each other, the obvious trend is more elastic strain in the pin as room temperature yield strength increases. The extreme point is the fictitious elastic SS calculation, which represents infinite yield strength. A simple explanation for this result is that the majority of the residual stresses are generated after the BMG completely "solidifies", since the pin–BMG interface should be able to transfer load to the pin. If the "solidification" or "setting" of the BMG is assumed to occur at 352 °C (its glass transition temperature), the maximum temperature at this instant at the center of the pin is only slightly higher (362 °C) according to the heat transfer solution. As mentioned earlier, the pin does not yield due to thermal gradients within itself before the "setting" of the BMG. Therefore, no significant high temperature plastic deformation is expected in the pin and the low temperature plastic properties of the SS essentially control the stress level in the pin. Indeed, when high temperature softening was deleted from the input file of Case 3 and the calculation was repeated, the results (not shown) were not significantly affected. This means, an accurate calculation of residual strains in the pin requires exact information about the plastic behavior of the SS only around room temperature. This result eliminates the influence on the final residual stresses of the high temperature constitutive behavior of the SS, an unknown in the present study. Although the exact heat treatment (and hence the room temperature plastic behavior) of the SS during the composite processing is not known, it can be reasonably speculated that it approaches Case 1 (i.e., yield strength around 200 MPa) judging from the proximity of the model predictions for this case to the ND data in the pin (Fig. 4).

Fig. 5 presents the axial residual stresses in the composite. The parabolic shape of the stress distribution in the BMG is typical of thermal tempering [3]. In Fig. 5, it is obvious that the stress profile in BMG is not influenced appreciably by the constitutive behavior of SS. Here, the temper level can be expressed as the difference between the end points of this parabola (∼560 MPa). In a tempered, monolithic BMG surface compression to mid-plane tension ratio is around 2 [6]. Hence, the temper level attained in the present study corresponds to about +190 MPa mid-plane tension and −380 MPa surface compression in a monolithic BMG sample. This result again proves that BMGs can build significant residual stresses due to thermal tempering. It is worth noting that the SS–BMG composite studied here is a tempered product, too,

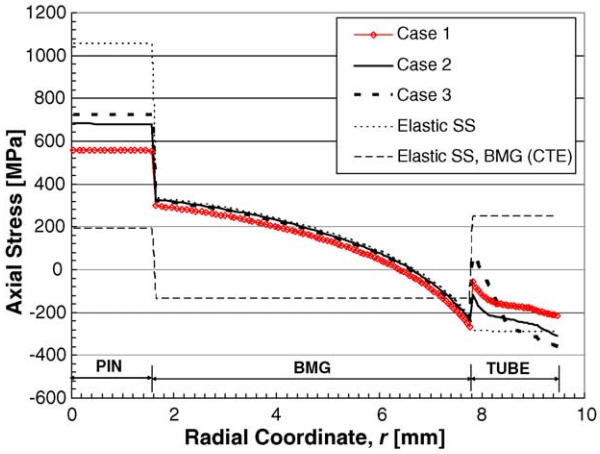

Fig. 5. Axial stresses predicted by the FE for various constitutive behaviors of SS and BMG (see the caption of Fig. 4 for details).

as the surface compressive axial stress in the SS tube reaches −200 MPa (Fig. 5).

The effect of the heat transfer coefficient on the final residual stresses was found to be minimal within the range of heat transfer coefficients studied: $h = 8000$–$10{,}000\ \mathrm{W/(m^2\,K)}$. Specifically, for Cases 1–3 the axial strain in the pin varied by less than 1%. Its variation was more pronounced (about 3%) for the "Elastic SS" case. This insensitivity is attributed to the saturation of the temper level at these high values of heat transfer coefficient [3,4].

Finally, it is important to note that there are other error sources in this thermomechanical problem whose solution is quite dependent on accurate information about material properties over a large temperature range (up to 900 °C). That means some of the discrepancy between model predictions and experimental data can be attributed to inaccurate material data. In addition, the viscoelastic theory for BMGs does not provide an exact description of their constitutive behavior because it disregards the structural relaxation in glass. In the previous study, the mid-plane tension and surface compression were overestimated by 15 and 30%, respectively [6]. This could be explained by the use of the equilibrium viscosity in calculations, which is higher than instantaneous viscosity around the glass transition of BMG when the glass relaxes [19]. In simple terms, this means the "solidification" temperature of the BMG was likely overestimated in the present analysis. As temperature gradients are decaying at this stage of the process, solidification at a lower temperature implies smaller temperature gradients. Since the bulk of tempering stresses are due to decay of temperature gradients after solidification [3,6], this means smaller residual stresses in reality. Hence, it is reasonable that the calculated elastic strain, which is linearly related to stress, was somewhat higher than the measurement as depicted in Fig. 4. The reader is referred to [6] for further details on the discrepancy between the thermoviscoelastic model predictions and experimentally measured residual stresses in BMGs.

5. Conclusions

A cylindrical stainless steel–bulk metallic glass composite was studied with an integrated analysis of neutron diffraction and finite element modeling. The diffraction data provided residual strain information in the SS components of the specimen while the finite element model allowed the interpretation of the data and the deduction of the stresses in both phases. A previously developed thermoviscoelastic model [5] was used to describe the constitutive behavior of the BMG while that of the SS was studied as a parameter in the finite element model. The following conclusions could be reached:

- Effective thermal tempering can be achieved in such a composite leading to high surface compression in the BMG (above −300 MPa) balanced with tension at the center.
- The strong bond between the SS and the BMG results in efficient load transfer and is critical in residual stress evolution during the quenching of the composite.
- The SS likely yields during processing. Its room temperature yield strength is estimated to be around 200 MPa. Although the processing initiates at high temperatures where the yield strength of the SS drops significantly, its constitutive behavior in this regime does not appreciably influence the final, room temperature residual stress state. This is due to the physics of the thermal tempering phenomenon, which is governed by the decay of temperature gradients below the glass transition of the BMG (around 350 °C in this case).
- The approach presented here can be employed in future evaluations of thermal tempering in BMGs using non-destructive stress measurement methods such as neutron diffraction. By combining the diffraction data from the SS with a mechanical model one can evaluate the extent of thermal tempering within reasonable accuracy.

Acknowledgement

This study is supported by the Center for Structural Amorphous Metals (Army Research Office Grant no. DAAD19-01-0525) at the California Institute of Technology.

References

[1] A. Peker, W.L. Johnson, Appl. Phys. Lett. 63 (1993) 2342.
[2] W.L. Johnson, JOM-J. Miner. Met. Mater. Soc. 54 (2002) 40.
[3] R. Gardon, in: R.D. Uhlmann, N.J. Kreidl (Eds.), Glass: Science and Technology, vol. 5, Academic Press, Orlando, FL, 1986, pp. 145–216.
[4] C.C. Aydiner, E. Ustundag, J.C. Hanan, Metall. Mater. Trans. A32 (2001) 2709.
[5] C.C. Aydiner, E. Ustundag, M.B. Prime, A. Peker, J. Non-Cryst. Solids 316 (2003) 82.
[6] C.C. Aydiner, E. Ustundag, Mech. Mater. 37 (2005) 201.
[7] D. Dragoi, E. Ustundag, B. Clausen, M.A.M. Bourke, Scripta Mater. 45 (2001) 245.
[8] B. Clausen, S.Y. Lee, E. Ustundag, C.C. Aydiner, R.D. Conner, M.A.M. Bourke, Scripta Mater. 49 (2003) 123.
[9] B. Clausen, S.Y. Lee, E. Ustundag, C.P. Kim, D.W. Brown, M.A.M. Bourke, Mater. Sci. Forum 404–407 (2002) 553.
[10] B. Clausen, S.Y. Lee, E. Ustundag, C.P. Kim, J.C. Hanan, D.W. Brown, M.A.M. Bourke, J. Appl. Phys. (2004).
[11] D.K. Balch, E. Ustundag, D.C. Dunand, J. Non-Cryst. Solids 317 (2003) 176.
[12] D.K. Balch, E. Ustundag, D.C. Dunand, Metall. Mater. Trans. 34A (2003) 1787.
[13] S.Y. Lee, B. Clausen, H. Choi-Yim, E. Ustundag, C.C. Aydiner, M.A.M. Bourke, Mater. Sci. Eng. A 399 (2005) 128.
[14] F.P. Incropera, D.P. DeWitt, Fundamentals of Heat and Mass Transfer, Wiley, New York, NY, 1996, p. 536.
[15] C.W. Tompson, D.F.R. Mildner, M. Mehregany, J. Sudol, R. Berliner, W.B. Yelon, J. Appl. Crystall. 17 (1984) 285.
[16] A.D. Krawitz, P.J. Rudnik, B.D. Butler, J.B. Cohen, Adv. X-Ray Anal. 29 (1986) 163.
[17] O.S. Narayanaswamy, J. Am. Ceram. Soc. 61 (1978) 146.
[18] E.H. Lee, T.G. Rogers, T.C. Woo, J. Amer. Ceram. Soc. 48 (1965) 480.
[19] T.A. Waniuk, R. Busch, A. Masuhr, W.L. Johnson, Acta Mater. 46 (1998) 5229.
[20] Metals Handbook, vol. 3, American Society for Metals, Metals Park, OH, 1978.
[21] W.F. Simmons, H.C. Cross, Report on Elevated Temperature Properties of Stainless Steels, American Society for Testing Materials, Philadelphia, PA, 1952.
[22] ABAQUS/Standard User's Manual, Version 6.3, Hibbitt, Karlsson & Sorensen Inc., 2002.
[23] R.D. Conner, R.B. Dandliker, W.L. Johnson, Acta Mater. 46 (1998) 6089.
[24] J. Lu, Ph.D. Thesis, California Institute of Technology, Pasadena, CA, 2002.
[25] W.L. Johnson, personal communication, 2003.
[26] R. Busch, Y.J. Kim, W.L. Johnson, J. Appl. Phys. 77 (1995) 4039.
[27] H.J. Fecht, Mater. Trans. JIM 36 (1995) 777.